Renewable Energy 256 (2026) 124743

Contents lists available at ScienceDirect

Renewable Energy

journal homepage: www.elsevier.com/locate/renene

# A benchmark simulator for advanced control of ethanol steam reforming

Mateo Arcila-Osorio [a,*], Francesco Destro [b], Carlos Ocampo-Martinez [a], Jordi Llorca [c], Richard D. Braatz [b]

[a] Automatic Control Department, Universitat Politècnica de Catalunya - BarcelonaTech, 08028, Barcelona, Spain
[b] Department of Chemical Engineering, Massachusetts Institute of Technology, MA 02139, Cambridge, USA
[c] Department of Chemical Engineering and Barcelona Research Center in Multiscale Science and Engineering, Universitat Politècnica de Catalunya - BarcelonaTech, 08019, Barcelona, Spain

ARTICLE INFO

*Keywords:*
Benchmark simulator
Ethanol steam reforming
Nonlinear dynamic modeling
Advanced control
Hydrogen production

ABSTRACT

This article presents a nonlinear dynamic simulator of an ethanol steam reforming process designed for pure hydrogen production for fuel-cell applications. The process consists of two stages: alcohol reforming and hydrogen separation within a staged-separation membrane reactor. The simulator is intended to serve as a benchmark for developing and testing advanced control, estimation, and optimization strategies. The simulator is extensively validated with experimental data. Detailed descriptions of the experimental setup, key modeling assumptions, and reference operating conditions are provided. Furthermore, critical control challenges that must be addressed to achieve optimal process operation are identified, along with quantitative metrics for evaluating the performance of control strategies implemented by users. A set of case studies illustrate the implementation of a proportional–integral–derivative (PID) controller in the benchmark simulator for tracking a hydrogen flow set-point and effectively rejecting disturbances. The benchmark simulator is developed in MATLAB® and is available in an online repository.

## 1. Introduction

Hydrogen is increasingly recognized as a versatile energy vector, capable of playing an essential role in the global transition to sustainable energy systems [1,2]. As a potential clean fuel, it offers a promising solution for decarbonizing sectors that are traditionally difficult to electrify, such as heavy industry, aviation, and transportation. The hydrogen's ability to store and transport energy makes it a flexible tool for balancing intermittent renewable energy sources like wind and solar. Moreover, hydrogen can be used as a feedstock in industrial processes, fuel for vehicles, or as a solution for short, medium, and long-term energy storage and short, medium, and long-range energy transfer [3,4]. However, the environmental impact of hydrogen production is highly dependent on the production method used [5,6]. Whereas conventional hydrogen production from fossil fuels (such as steam methane reforming [7]) is carbon intensive, alternative methods, such as water electrolysis powered by renewable energy and alcohol steam reforming (ASR), among others, offer more sustainable pathways to hydrogen production [8]. The latter is of especial interest, especially in regions where biomass or bio-alcohols are readily available [9].

Water electrolysis, the most widely studied method for clean hydrogen production, splits water into hydrogen and oxygen using an electric current [10]. When this process is powered by renewable sources such as solar, wind, or hydropower, the hydrogen produced is considered *green* due to its minimal environmental impact [11]. Advances in electrolysis technologies, such as proton exchange membranes (PEM) and solid oxide electrolysis cells (SOEC), have made the production of green hydrogen more efficient and economically attractive. However, additional challenges related to durability, performance, cost, energy efficiency, and scalability remain significant barriers to the widespread adoption of such a hydrogen production technique [12,13].

On the other hand, ASR involves the catalytic conversion of alcohols (typically methanol or ethanol) and water into hydrogen and some byproducts (carbon monoxide, carbon dioxide, methane, among others) at high temperatures [14,15]. Ethanol production pathways vary significantly depending on the feedstock. While ethanol is often produced from fossil-derived ethylene through chemical conversion, this study focuses on ethanol obtained from renewable biomass sources, such as corn, sugarcane, or lignocellulosic materials, commonly referred to as bio-ethanol [16,17]. In this context, the ethanol steam reforming (ESR) process aligns with the principles of green hydrogen production [18,19]. Hydrogen derived from biomass can be considered carbon-neutral,

* Corresponding author.
*E-mail addresses:* mateo.arcila@upc.edu (M. Arcila-Osorio), destro@mit.edu (F. Destro), carlos.ocampo@upc.edu (C. Ocampo-Martinez), jordi.llorca@upc.edu (J. Llorca), braatz@mit.edu (R.D. Braatz).

https://doi.org/10.1016/j.renene.2025.124743
Received 3 May 2025; Received in revised form 10 September 2025; Accepted 8 November 2025
Available online 10 November 2025

even without carbon capture technologies, since the carbon dioxide released during reforming comes from carbon previously captured by plants during growth [20]. To further enhance sustainability, the energy input should also originate from renewable sources, and the carbon dioxide generated can be minimized or captured, as the method proposed in [21]. Similarly, the reduction of process byproducts can be achieved through the appropriate application of advanced control and optimization strategies. Alcohol reforming offers several advantages, such as the use of renewable feedstock and a lower carbon footprint compared to traditional fossil-fuel-based methods. Additionally, ASR can be more relevant than electrolysis in regions lacking abundant renewable electricity, making it an attractive option for decentralized hydrogen production.

The suitable implementation of ASR for clean hydrogen production requires the development of efficient and robust control strategies to maintain optimal operation while ensuring the hydrogen purity despite the presence of uncertainty. This purity is essential for the successful integration of these devices into complex smart grids for clean energy generation. Despite this need, there is limited research on the optimal design of model-based control strategies for alcohol reformers. Many existing studies primarily focus on steady-state behavior, employing simple control loops and neglecting both physical limitations and operational constraints [22,23]. Other research focus on developing predictive controllers to regulate hydrogen outflow, incorporating constraints related to inputs, states, and outputs [24,25]. However, these studies depend on linear process models, which often exhibit limited accuracy and reliability in a wide operating range of the device. Another study [26] analyzed the nonlinear dynamics for a physics-based distributed parameter model for an ethanol steam reformer, highlighting the complexity of the proposed model in terms of nonlinearities and variable interactions. Nonetheless, this work did not propose or address any specific control strategy. On the other hand, data-driven approaches, such as artificial neural networks, have been used for catalyst selection [27], experimental analysis [28], and process modeling and optimization [29,30]. However, despite their relevant predictive capabilities, these approaches require extensive experimental datasets for model training, and offer limited interpretability of the underlying physical and chemical phenomena.

The discussed studies and others found in the literature propose various models and test different control strategies. However, they often lack a detailed description of the system, including a real experimental setup and the typical operating conditions. As a result, comparing the performance of controllers is challenging without a common framework. This issue is further compounded by the wide variety of control strategies available, which require proper evaluation and comparison under consistent conditions. Successful examples of benchmark simulators of physical–chemical systems have shown how a well-documented, dynamic, and physically grounded framework enables fair and reproducible comparison of process monitoring, control, and optimization strategies. For instance, the Tennessee Eastman benchmark [31] was a pioneering challenging problem for a wide variety of process control studies and remains one of the most widely used benchmarks in process systems engineering. The work in [32] presents a validated industrial-scale penicillin fermentation simulator, developed from mechanistic models and historical plant data, which serves as a realistic benchmark for process systems analysis and control studies. Likewise, ContCarSim, a validated mechanistic simulator of continuous intensified filtration–drying on carousel technology is presented in [33], providing a benchmark for quality-by-design and quality-by-control strategies and supporting the transition toward end-to-end continuous pharmaceutical manufacturing. Moreover, [34] provides a comprehensive review and comparison of openly available benchmark simulators and datasets, offering guidance on their suitability for process monitoring, fault diagnosis, and scientific advancement. While these and many others tools address relevant research fields, no openly accessible benchmark simulator exists within the context of sustainable hydrogen production. Without such a common reference, comparing the performance of diverse algorithms remains challenging, as each study operates under its own conditions, assumptions, datasets, and disturbance scenarios.

The main contribution of this article is to provide a benchmark simulator of an ESR process within a staged-separation membrane reactor (SSMR). Such a process is represented by a mechanistic dynamic mathematical model. The model describes a complex physical–chemical process characterized by highly coupled nonlinear dynamics, which presents significant challenges for state estimation and control design. A real SSMR setup is considered, which was used to run experiments and estimate the model parameters. Besides, control challenges relevant to this process are presented, and case studies demonstrate the implementation of a closed-loop control system within the benchmark framework. The benchmark is publicly available and supports the optimization of ESR/SSMR operation in terms of both economic and environmental impact, by enabling in silico evaluation of control, monitoring, and optimization algorithms, while also serving as a valuable educational tool.

The remainder of this article is organized as follows: Section 2 details the process description and experimental setup. Section 3 presents the SSMR mathematical model and its validation. Section 4 describes the benchmark simulator with the main operational considerations. Section 5 discusses sample case studies. Finally, the conclusions of this work are drawn in Section 6.

## 2. Process description

The process considered in this article involves the catalytic transformation of gaseous ethanol and steam into hydrogen and waste gases, namely, an ESR process. The entire process integrates two unit operations in series: (*i*) a reforming stage and (*ii*) a separation stage within a SSMR. In the reforming stage, ethanol and steam are fed into a tubular monolithic reactor with catalytic walls where chemical reactions occur as the reactants move through the device. The reactor walls (cordierite monoliths) are functionalized with a cobalt-based ($Co_3O_4$-ZnO) catalyst layer, which promotes the desired reactions at relatively low temperatures. Since fuel cells require high-purity hydrogen, this component is isolated in the separation stage of the SSMR. In this way, the pure hydrogen is obtained on the permeate side of a palladium-silver (Pd-Ag) membrane, while the waste products remain on the retentate side. No chemical reactions occur in this separation stage.

Commonly, SSMRs can have different dimensions and configurations according to the specific application, e.g., [35]. The schematic representation of the experimental SSMR setup considered in this study is shown in Fig. 1. The operational zone of the device has a total length of 23.0 cm, with 15.4 cm allocated to the reforming stage and the remaining 7.6 cm corresponding to the separation stage (membrane length). Both stages have the same outside diameter of 2.2 cm. The reactive zone is loaded with a total of 1.32 g of the cobalt-based catalyst. In addition, the membrane is a 1/8 inch diameter, pinhole-free, dead-end membrane tube with a total area of 7.1 $cm^2$ and a Pd-Ag active layer of 30 μm thick over a layer of appropriate support. The reaction scheme [36] that occurs in the reforming stage of the process is

$$C_2H_5OH \longrightarrow CH_3CHO + H_2, \tag{1a}$$

$$C_2H_5OH \longrightarrow CO + CH_4 + H_2, \tag{1b}$$

$$CO + H_2O \rightleftharpoons CO_2 + H_2, \tag{1c}$$

$$CH_3CHO + 3\,H_2O \longrightarrow 2\,CO_2 + 5\,H_2, \tag{1d}$$

where ethanol undergoes either dehydrogenation into acetaldehyde and hydrogen over cobalt oxide (1a) or decomposition into carbon monoxide, methane, and hydrogen through an undesired reaction (1b). Cobalt-based catalysts are also active for the water-gas shift reaction (1c) under typical operating conditions. Finally, the main reaction

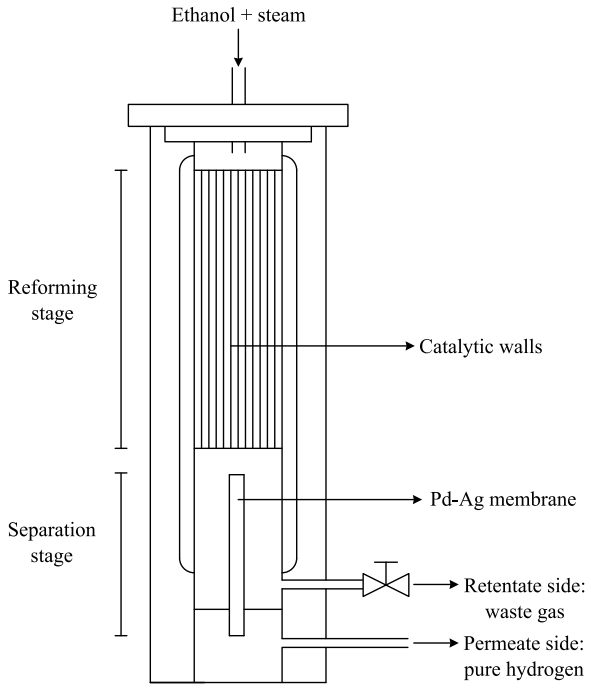


**Fig. 1.** Schematic representation of the staged-separation membrane reactor (SSMR).

occurs in which acetaldehyde is reformed with water to produce carbon dioxide and hydrogen over metallic cobalt (1d).

On the other hand, a simple schematic diagram of the complete unit for pure hydrogen production is shown in Fig. 2. The liquid ethanol and liquid water are fed directly from the storage tanks using HPLC pumps. This mixture is then vaporized as it passes through a heating conduit before entering the SSMR. There, chemical reactions and hydrogen separation through the membrane take place. The retentate pressure is controlled and adjusted to different values, while the permeate side is maintained at atmospheric pressure without any pressure regulation [37]. The benchmark includes standard symbols for instrumentation such as temperature, pressure, and flow indicators. However, users are encouraged to add additional elements, including controllers, to design and test their control strategies. This flexibility allows for a range of control approaches, from basic loops to advanced model-based techniques.

## 3. Mathematical model

The mathematical model is developed building on previously developed ESR models [25,26], which addressed the same experimental setup. Accurately modeling the process is challenging due to the strong interactions among simultaneous phenomena such as chemical reactions, mass transfer, and heat transfer, leading to high coupling of variables. Nevertheless, the model can be simplified without sacrificing accuracy or reliability by the assumptions

**A1.** The concentrations in the SSMR can be effectively represented by two plug-flow units in series: a tubular reactor followed by a tubular membrane separator. The fundamental assumption of plug-flow behavior is that the fluid is perfectly mixed in the radial direction but not in the axial direction (forwards or backwards), with each plug having a different composition from the ones before and after it.

**A2.** Radial variations in pressure and temperature are negligible in both the tubular reactor and membrane separator. This assumption is justified by the minimal flow or friction in the radial direction and the short radial length scale relative to the axial direction.

**A3.** The dependence of the velocity in the radial direction is also neglected. Instead, the fluid velocity is taken to be the average radial velocity at any specific point along the reactor.

**A4.** The ideal gas equation is valid for the operating pressure range in the device, that is, $P(V/n) = RT$, where $P$ is the gas pressure, $V/n$ is the molar gas volume, $R$ is the universal gas constant, and $T$ is the gas temperature. The relatively low pressures in the process support this assumption.

**A5.** Axial molecular diffusion effects are negligible compared to axial convection. This assumption is validated by calculating the Péclet number, which is the ratio of the reactor characteristic length and flow velocity to the molecular diffusivity. A high Péclet number, typical in most industrial applications, justifies omitting second-order spatial derivative terms related to the axial direction in the modeling equations.

Based on the above assumptions, the mathematical model for the two process units depends on both time and the axial direction along the SSMR. As a result, the model consists of a set of nonlinear partial differential equations (PDEs) that describe the dynamic behavior of the system. The model parameters are either taken directly or adapted from [25,36] and summarized in Appendix A. The model predicts the species concentrations and gas mixture temperature as the gas mixture flows through the device. For control purposes, the focus is on the outlet gas mixture composition and flow rate, which are crucial for efficiently feeding fuel cells and ensuring optimal energy production.

### 3.1. Reforming stage

The equations representing the mass conservation principle in the reforming stage for the seven $j \in \{1, 2, \dots, 7\}$ species ($C_2H_5OH$, $H_2O$, $CH_4$, $H_2$, CO, $CO_2$, $CH_3CHO$) are expressed, with initial and boundary conditions, as

$$\frac{\partial C_j}{\partial t} + \frac{\partial (v C_j)}{\partial z} = \sum_{i=1}^{4} \nu_{j,i} r_i, \tag{2a}$$

$$C_j(0, z) = C_{j,0}(z), \quad \forall z \in [0, \ell_1], \tag{2b}$$

$$C_j(t, 0) = C_{j,\text{in}}(t), \quad \forall t \geq 0, \tag{2c}$$

where

- $C_j$ is the concentration (mol/m$^3$) of the $j$th species,
- $v$ is the linear velocity (m/min) of the gas mixture in the axial direction and can be estimated based on the input molar flow rates and reaction rates using

$$v = \frac{RT}{PA}\left(\sum_{j=1}^{7} F_{j,\text{in}} + \sum_{i=1}^{4} \int \chi_i r_i dV\right), \tag{3}$$

- $t$ and $z$ are the time (min) and axial position (m), respectively,
- $R$ is the gas universal constant (J/(mol K)),
- $T$ is the gas mixture temperature (K),
- $P$ is the gas mixture pressure (Pa),
- $A$ is the cross-sectional area (m$^2$),
- $F_{j,\text{in}}$ is the inlet molar flow rate (mol/min) of the $j$th species (manipulated variable),
- $i \in \{a, b, c, d\}$ is the reaction index, with reference to chemical reactions (1a)–(1d),
- $\chi_i$ is a coefficient indicating the change in moles in the $i$th chemical reaction,
- $r_i$ is the reaction rate (mol/(m$^3$ min)) of the $i$th chemical reaction,
- $V$ is the volume (m$^3$) of the analyzed reactor section,
- $\nu_{j,i}$ is the stoichiometric coefficient (dimensionless) of the $j$th species in the $i$th reaction,

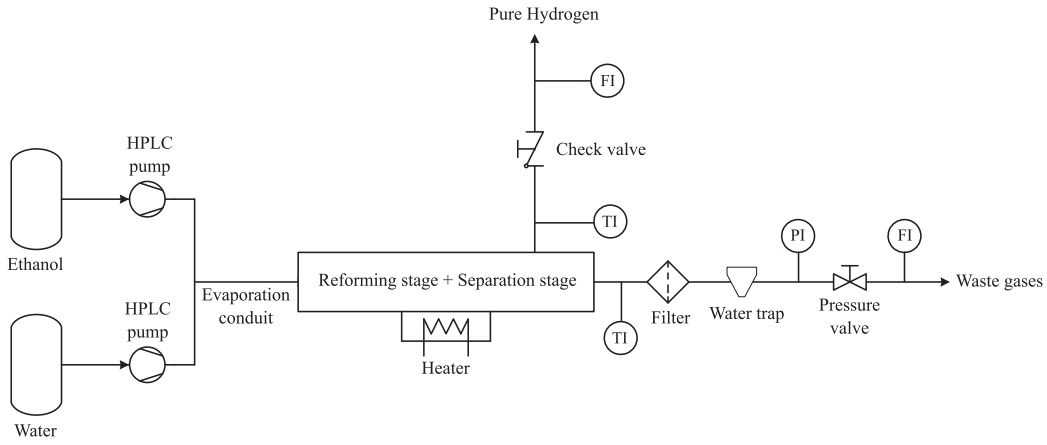


**Fig. 2.** Schematic diagram of the ethanol steam reforming (ESR) process for pure hydrogen production.
*Source:* Adapted from [37].

- $C_{j,0}(z)$ is the concentration of the $j$th species at time $t = 0$ along the reactor,
- $C_{j,\text{in}}(t)$ is the inlet concentration (mol/m$^3$) of the $j$th species over time and can be calculated as

$$C_{j,\text{in}}(t) = \frac{F_{j,\text{in}}(t)}{F_{T,\text{in}}(t)} \frac{P}{RT_{\text{in}}(t)}, \tag{4}$$

- $F_{T,\text{in}}(t)$ is the total inlet molar flow rate (mol/min) over time,
- $T_{\text{in}}(t)$ is the gas mixture inlet temperature (K) over time, and
- $\ell_1$ is the axial length (m) of the reforming stage.

The reaction rates are given by[1]

$$r_a = k_a \frac{P_{C_2H_5OH}}{\alpha_a + \beta_a(\frac{P}{10^5} - 1)}, \tag{5a}$$

$$r_b = k_b P_{C_2H_5OH}, \tag{5b}$$

$$r_c = k_c \left( P_{CO} P_{H_2O} - \frac{P_{CO_2} P_{H_2}}{k_{WGS}} \right), \tag{5c}$$

$$r_d = k_d P_{CH_3CHO} P_{H_2O}^3, \tag{5d}$$

$$k_{WGS} = \exp\left(\frac{4577.8}{T} - 4.33\right), \tag{5e}$$

$$k_i = k_{\infty,i} \exp\left(-E_{a,i}\left(\frac{1}{RT} - \frac{1}{RT_{\text{ref}}}\right)\right), \tag{5f}$$

in which

- $k_i$ is the kinetic parameter of the $i$th chemical reaction,
- $\alpha_a$ and $\beta_a$ are parameters accounting for equilibrium effects in reaction rate (5a),
- $P_j$ is the partial pressure (bar) of the $j$th species ($P_j = C_j RT$),
- $k_{WGS}$ is a parameter of the water–gas shift reaction,
- $k_{\infty,i}$ is the pre-exponential factor of the $i$th kinetic parameter,
- $E_{a,i}$ is the activation energy (J/mol) of the $i$th chemical reaction, and
- $T_{\text{ref}}$ is the reference temperature for the reaction rates, which is equal to 773 K.

The energy balance for the reforming stage is

$$\sum_{j=1}^{7} C_{v,j} C_j \frac{\partial T}{\partial t} = Ua(T_a - T) - \sum_{i=1}^{4} \Delta H_i r_i - \sum_{j=1}^{7} C_{p,j} C_j v \frac{\partial T}{\partial z}, \tag{6a}$$

$$T(0, z) = T_0(z), \quad \forall z \in [0, \ell_1], \tag{6b}$$

$$T(t, 0) = T_{\text{in}}(t), \quad \forall t \geq 0, \tag{6c}$$

where

- $T_0(z)$ is the temperature profile at time $t = 0$ along the reactor,
- $T_{\text{in}}(t)$ is the inlet temperature of the gas mixture over the time,
- $C_{v,j}$ is the heat capacity (J/(mol K)) at constant volume of the $j$th species,
- $U$ is the global heat transfer coefficient (J/(m$^2$ min K)),
- $a$ is the area per volume of reactor (m$^2$/m$^3$) where heat is being interchanged,
- $T_a$ is the furnace temperature (K),
- $C_{p,j}$ is the heat capacity (J/(mol K)) at constant pressure of the $j$th species,
- $\Delta H_i$ (J/mol) is the molar heat of reaction $i$, which is given by

$$\Delta H_i = \Delta H_i^\circ + \Delta C_{Pi} (T - 298), \tag{7}$$

with $\Delta H_i^\circ$ being the molar heat of reaction $i$ at standard conditions (298 K, 1 bar), and
- $\Delta C_{Pi}$ denotes the difference between the heat capacities of products and reactants in reaction $i$. Note that in (6a) the change in heat capacities with temperature is neglected.

### 3.2. Separation stage

Formulating the mass balance for the separation stage requires modeling the mass transfer across the membrane. Since the separation stage does not contain a catalyst, the effect of chemical reactions is negligible in this compartment of the SSMR. The mass balances of the seven components of the gas mixture in the separation stage are

$$\frac{\partial C_j}{\partial t} + \frac{\partial (vC_j)}{\partial z} = F_j, \tag{8}$$

where $F_j$ is the flow rate of species $j$ through the membrane. Boundary conditions are determined by the continuity of flow rates between the reforming outlet and the separation inlet. The flow rate through the membrane is equal to zero for all components, except for hydrogen. The hydrogen permeation process is described by Sieverts' Law [38], i.e.,

$$F_{H_2} = \frac{P_e}{\delta} \alpha \left( \sqrt{P_{H_2,r}} - \sqrt{P_{H_2,p}} \right), \tag{9a}$$

$$P_e = P_{e,0} \exp\left(\frac{-E_{am}}{RT}\right), \tag{9b}$$

where

[1] In this work, (5a) was modified to account for the effect of the operating pressure. Specifically, an additional term was introduced in the denominator compared to the original equation from [36].

- $F_{H_2}$ is the hydrogen molar flow rate (mol/min) that permeates through the membrane,
- $P_e$ is the permeability (mol/(m min $Pa^{1/2}$)) of the membrane,
- $P_{e,0}$ is the permeability (mol/(m min $Pa^{1/2}$)) pre-exponential factor,
- $\delta$ is the membrane thickness (m),
- $\alpha$ is the surface area of the membrane ($m^2$),
- $P_{H_2,r}$ and $P_{H_2,p}$ are the hydrogen partial pressures (Pa) at the retentate and permeate sides, respectively, and
- $E_{am}$ is the apparent activation energy of the membrane (J/mol).

The parameters $P_e$, $P_{e,0}$, $\delta$, $\alpha$, and $E_{am}$ have been adjusted based on experimental data collected on a real SSMR by employing the methodology detailed in [25]. Finally, the energy balance equation for the separation stage is similar to that of the reforming stage, but it neglects temperature changes from chemical reactions and adds a term to account for energy loss due to hydrogen permeation, i.e.,

$$\sum_{j=1}^{7} C_{v,j} C_j \frac{\partial T}{\partial t} = U a (T_a - T) - \sum_{j=1}^{7} C_{p,j} C_j v \frac{\partial T}{\partial z} - F_{H_2,\mathrm{vol}} \overline{U}_{H_2}, \tag{10a}$$

$$T(0, z) = T_0(z), \quad \forall z \in [\ell_1, \ell_2], \tag{10b}$$

$$T(t, 0) = T_{\mathrm{in}}(t), \quad \forall t \geq 0, \tag{10c}$$

where

- $F_{H_2,\mathrm{vol}}$ is the hydrogen molar flow rate (mol/(min $m^3$)) per unit volume that permeates through the membrane,
- $\overline{U}_{H_2}$ is the molar internal energy (J/mol) of hydrogen,
- $T_0(z)$ is the temperature profile at time $t = 0$ along the separation stage,
- $T_{\mathrm{in}}(t)$ is the separation stage inlet (reforming stage outlet) temperature of the gas mixture over the time, and
- $\ell_2$ is the axial length (m) of the separation stage.

### 3.3. Model simulation and validation

To numerically simulate the process model, the spatial derivatives of the states (concentrations and temperature) are approximated using a first-order finite difference upwind scheme [39], i.e.,

$$\frac{\partial x}{\partial z} \approx \frac{x(k) - x(k-1)}{\Delta z}, \tag{11}$$

where $x$ is the corresponding state, $k$ is the discrete time step, and $\Delta z$ is the distance between two spatial discretization points. By applying this technique, the PDEs of the model can be transformed into a set of ordinary differential equations (ODEs) along several spatial discretization points, which are then solved with `ode15s` in MATLAB®. All simulations reported in this paper were performed using MATLAB® R2023a on a laptop equipped with an AMD Ryzen 5 3500U processor with Radeon Vega Mobile Graphics (2.10 GHz) and a total memory of 8.0 GB RAM.

The experimental procedure follows the methodology described in [40], with modifications to suit the current system configuration. A liquid mixture of ethanol and water, prepared to achieve a specific steam-to-carbon ($S/C$) ratio, is supplied directly from a storage tank using a Knauer smartline pump. Before entering the SSMR, the mixture is vaporized via a heated conduit, bringing it to the same temperature as the reactor walls. The reactor temperature is controlled using an electrical resistance heater regulated by propotional–integral–derivative (PID) electronic controller (Fuji PXR4) and insulated with glass wool. A K-type thermocouple positioned in direct contact with the membrane surface ensures accurate temperature monitoring.

On the retentate side of the SSMR, a liquid trap is installed to condense and collect any non-gaseous components. The system pressure on this side is controlled and adjusted with a manually-operated back pressure regulation, allowing operation under different steady-state pressure conditions. The permeate side remains open to the atmosphere, with no additional pressure regulation. The product gas compositions from both the retentate and permeate streams are analyzed by using an online gas chromatograph (Agilent 3000 A MicroGC) equipped with MS 5 Å, Plot U, and Stabilwax columns. The hydrogen flow rate at the permeate side was quantified using an electronic mass flow meter (Bronkhorst), while the volumetric flow rate of the retentate stream is measured with a soap bubble meter. A series of steady-state experiments were conducted by systematically varying the retentate pressure, while keeping constant inlet volumetric flow, $S/C$ ratio, temperature and catalyst load. Each operating condition was held until steady state was confirmed through stable concentration profiles in the chromatographic measurements.

Model validation was performed by comparing simulation results with experimental data under steady-state conditions. The experiments were conducted at $S/C$ ratio of 2.4, a temperature of 500 °C, and various pressures. These conditions correspond to an inlet ethanol molar flow of 0.0021 mol/min and an inlet water molar flow of 0.0099 mol/min. The kinetic parameters $\alpha_a$ and $\beta_a$ from reaction rate (5a), along with the permeability pre-exponential factor $P_{e,0}$, were estimated by solving a sequential quadratic programming (SQP) problem aimed at minimizing the sum of squared errors across multiple species, framing the task as a multiobjective optimization problem. The model was trained using experimental data at 8 and 10 bar, while data at 1, 4, 6, 12, and 14 bar were reserved for validation. As shown in Fig. 3, the simulation results show excellent agreement with the experimental measurements across different pressures, for both training and validation experiments.

Although the model was successfully validated with experimental data, the following limitations should be considered when using the simulator. The model adopts a plug-flow representation with negligible axial dispersion and no radial gradients. This assumption may be inaccurate for large-diameter reactors, strongly exothermic or endothermic operation, nonuniform inlet distributions, or regimes with significant radial heat or mass transfer resistances. Further, catalyst activity and membrane permeability could be treated as run-invariant parameters in the configurations reported here (i.e., no explicit deactivation, fouling, or aging kinetics), which may underpredict long-run drift. In addition, the present release is deterministic: stochastic disturbances (e.g., sensor noise, feed fluctuations) are not explicitly modeled. Finally, an ideal-gas equation of state is assumed within the studied operating window; non-ideal behavior may require correction at higher pressures or lower temperatures.

## 4. Benchmark simulator description

### 4.1. Simulator input/output structure

Running an open-loop simulation requires specifying the inputs:

- Gas inlet temperature, $T_{\mathrm{in}}$ (between 500 and 600 °C)
- Gas inlet pressure, $P_{\mathrm{in}}$ (between 1 and 14 bar)
- Inlet ethanol molar flow rate, $u_1$ (between 0.0018 and 0.0024 mol/min)
- Inlet water molar flow rate, $u_2$ (between 0.0087 and 0.0108 mol/min)
- Simulation duration, $t$ (min)
- Initial conditions: axial profiles of species concentration and gas mixture temperature. Two default initial conditions scenarios are implemented in the simulator (see Table 1).

Table 2 presents simulation inputs for three representative scenarios of normal operating conditions in the SSMR. For running a closed-loop simulation, the same inputs as in the open-loop case must be specified, except for the manipulated variables $u_1$ and $u_2$, which are, instead, dynamically adjusted by the controller using user-defined control laws. On the other hand, the simulation outputs are

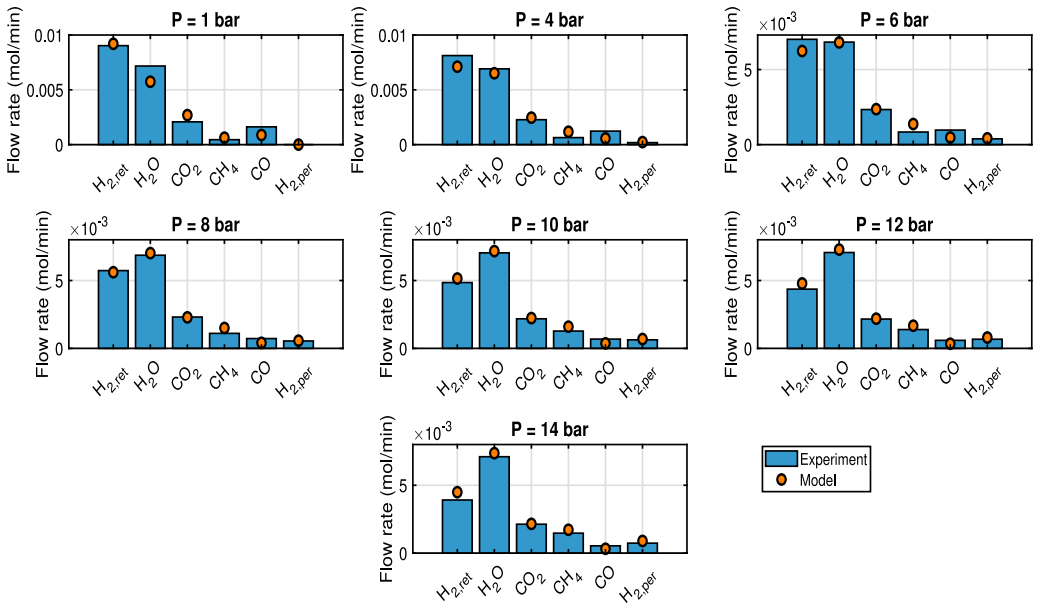


**Fig. 3.** Model validation. Model predictions and experimental measurements are compared for the outlet flow rates of the species at different pressures. Ethanol and acetaldehyde flows are not shown, since they are fully consumed.

**Table 1**
Default initial conditions scenarios implemented in the simulator.

| Scenario | Initial conditions |
|---|---|
| 0 | Axial profiles of species concentration and temperature |
| 1 | Reactor filled with only steam with uniform temperature |

- *Simulated measurements*. These simulation outputs represent the measurements that can be obtained from physical sensors or instruments during real-world operation of the SSMR, i.e.,
  - outlet volumetric flow rate of waste gas, $Q_w$,
  - outlet volumetric flow rate of pure hydrogen, $Q_{\mathrm{H}_2}$,
  - outlet waste gases concentration, $C_{j,\mathrm{out}}$, and
  - gas outlet temperature, $T_{\mathrm{out}}$.
- *System states*. These outputs include the gas temperature and concentration profiles along the device, providing deeper insights into the process dynamics beyond what can be observed in practice.

The structure of the simulation outputs helps to distinguish between the data available for monitoring and control in real-world scenarios and additional insights provided by the simulation to support analysis and decision-making tasks.

### 4.2. Disturbance scenarios

Disturbance scenarios are implemented in the simulator to evaluate control strategies under realistic disturbance conditions. The sources of process variability in the SSMR come primarily from fluctuations in the gas inlet conditions, such as pressure and temperature, as well as from longer-term issues like catalyst deactivation and separation membrane fouling. Disturbances in the gas inlet conditions can occur due to external factors such as feedstock inconsistencies or operational adjustments, directly impacting the process performance. Catalyst deactivation, a common phenomenon in chemical processes, gradually reduces the efficiency of reactions, typically due to poisoning, sintering, or coking. Similarly, membrane fouling, which arises from the accumulation of contaminants on the membrane surface or within its pores, leads to a decline in separation efficiency and an increase in energy requirements.

In the simulator, the disturbance scenarios are implemented through the parametric step changes or drifts:

1. *Disturbance scenario 1*: A ± 10% step change in the gas inlet temperature (in K).
2. *Disturbance scenario 2*: A ± 20% step change in the gas inlet pressure.
3. *Disturbance scenario 3*: To simulate catalyst deactivation, all kinetic parameters of the chemical reactions are multiplied by a decreasing exponential factor over time, i.e.,

   $$k_{i,\mathrm{new}} = k_i \exp(-\beta t),$$

   where $\beta$ is a parameter that influences the time required for complete deactivation of the catalyst.
4. *Disturbance scenario 4*: To simulate membrane fouling, the membrane permeability is multiplied by a decreasing exponential factor over time, as follows:

   $$P_{e,\mathrm{new}} = P_e \exp(-\alpha t),$$

   where $\alpha$ is a parameter that modulates the time required for the complete fouling of the membrane and, therefore, the total obstruction of the flow of pure hydrogen.

### 4.3. Control challenges

Control challenges that reflect real-world scenarios arising in ESR operation are

1. *Ensuring outlet pure hydrogen flow rate*. This challenge consists of tracking the set-point profile 1 of outlet hydrogen flow rate reported in Fig. 4, starting from Mode 1 of normal operating conditions and scenario 0 of initial conditions. Tracking this set-point profile is the primary control objective of the SSMR, since the profile represents the hydrogen demand profile from a downstream fuel cell.
2. *Reducing ethanol consumption*. This challenge consists of minimizing ethanol consumption, while simultaneously tracking the set-point profile 1 of Fig. 4, starting from Mode 1 of normal operating conditions and scenario 0 of initial conditions.

**Table 2**
Input values of proposed normal operating conditions.

| Parameter | Symbol | Units | Mode 1 | Mode 2 | Mode 3 |
|---|---|---|---|---|---|
| Inlet ethanol molar flow | $u_1$ | mol/min | 0.0021 | 0.0018 | 0.0024 |
| Inlet water molar flow | $u_2$ | mol/min | 0.0099 | 0.0108 | 0.0088 |
| Gas inlet temperature | $T_{in}$ | K | 773.15 | 823.15 | 873.15 |
| Gas inlet pressure | $P_{in}$ | bar | 4.0 | 6.0 | 8.0 |

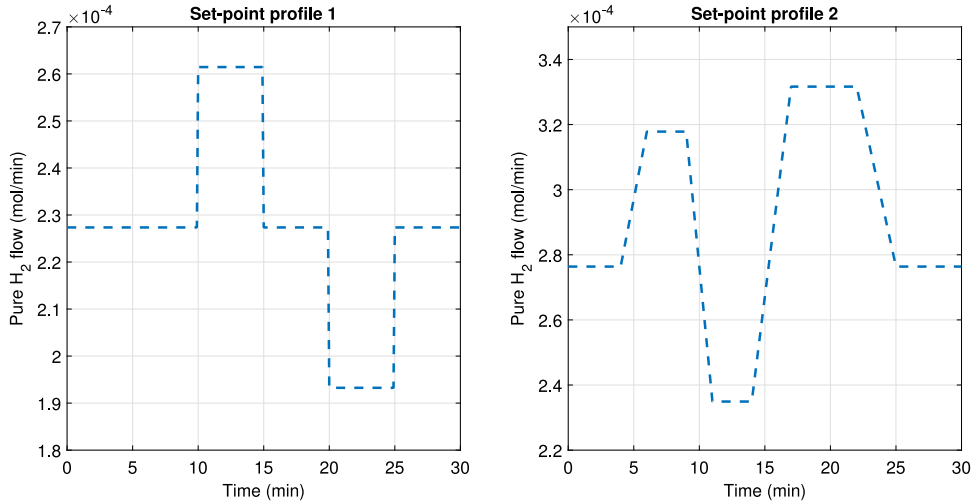


**Fig. 4.** Set-point profiles of outlet hydrogen flow rate for control challenges.

3. *Handling fluctuations in gas inlet conditions*. This challenge consists of tracking a constant set-point value, in disturbance scenario 1 or 2, and starting from Mode 2 of normal operating conditions and scenario 1 of initial conditions.
4. *Compensating for catalyst deactivation*. This challenge consists of tracking the set-point profile 2 of Fig. 4, in disturbance scenario 3, and starting from Mode 2 of normal operating conditions and scenario 0 of initial conditions. This control challenge is harder than the previous one, since the catalyst activity is not measured.
5. *Managing membrane fouling in hydrogen separation*. This challenge consists of tracking the set-point profile 2 of Fig. 4, in disturbance scenario 4, and starting from Mode 2 of normal operating conditions and scenario 0 of initial conditions. As for catalyst deactivation, membrane permeability is not a parameter that is measured in real-time.
6. *Minimizing energy consumption*. The process involves high temperatures and pressures, which can lead to significant energy consumption. This challenge consists of tracking the set-point profile 2 of Fig. 4, free of disturbances, and starting from Mode 3 of normal operating conditions and scenario 1 of initial conditions. For this control challenge, it is possible to manipulate the reactor wall temperature.

Table 3 provides a summary of the simulation conditions associated with the outlined control challenges. Quantitative metrics to assess the performance of the proposed control systems are also suggested. Users are encouraged to explore their own combinations of control challenges, disturbance scenarios, normal operating conditions, initial conditions, and performance metrics to tailor the benchmark to their specific needs.

## 5. Case studies

The case studies are presented to illustrate a straightforward application of the benchmark simulator. Therefore, two basic control challenges are addressed to demonstrate relatively suitable performance without requiring the design of advanced control strategies. The latter are left for future work and for users to explore and implement.

### 5.1. Case study 1

This case study consists of the implementation of a simple controller in the simulator to address control challenge 1. First, to analyze the system dynamic response, an input step change was simulated. The system was run in open loop under Mode 1 of normal operating conditions. After 2 min of simulation, a change in the inlet ethanol molar flow was introduced, increasing from 0.0021 to 0.0024 mol/min. Fig. 5 presents the system dynamic response, illustrating the outlet molar flow of pure hydrogen. Such a system response exhibits a dead time of around 0.15 min and a time constant of 0.25 min. For reference, simulating the process over 4 min of operation time and with a total of 100 spatial discretization points took approximately 20 s on the specified laptop.

Control challenge 1 could resemble a small-scale hydrogen generation unit supplying a low-power fuel cell for auxiliary or backup power in a microgrid, where hydrogen demand fluctuates due to varying electricity consumption patterns, intermittent renewable generation, and load changes. To explore this scenario, a PID controller to regulate pure hydrogen production is implemented. The inlet ethanol molar flow serves as the manipulated variable, directly affecting hydrogen generation. Since a buffer storage is not assumed, the system must respond rapidly to the demand changes without relying on stored hydrogen reserves.

The controller is implemented in the standard discrete form,

$$F_{\mathrm{EtOH}}(k) = K_p e(k) + K_i \sum_{j=0}^{k} e(j) T_s + K_d \frac{e(k) - e(k-1)}{T_s}, \tag{12a}$$

$$e(k) = F_{\mathrm{H_2}}^{\mathrm{sp}}(k) - F_{\mathrm{H_2}}(k), \tag{12b}$$

where

- $F_{\mathrm{EtOH}}(k)$ is the manipulated variable, corresponding to the inlet ethanol molar flow (mol/min) at time step $k$,
- $e(k)$ is the control error (mol/min) at time step $k$, defined as the difference between the desired hydrogen production rate (set-point) $F_{\mathrm{H_2}}^{\mathrm{sp}}(k)$, and the measured hydrogen permeate flow $F_{\mathrm{H_2}}(k)$,

**Table 3**
Simulation conditions associated with the outlined control challenges.

| Control challenge | Performance metric | Disturbance scenario | Operating conditions | Initial conditions |
|---|---|---|---|---|
| 1 | IAE with respect to the set-point profile | Free of disturbances | Mode 1 | Scenario 0 |
| 2 | Percentage of reduction in ethanol consumption relative to Control Challenge 1 | Free of disturbances | Mode 1 | Scenario 0 |
| 3 | IAE with respect to the constant set-point value | 1 or 2 | Mode 2 | Scenario 1 |
| 4 | IAE with respect to the set-point profile | 3 | Mode 2 | Scenario 0 |
| 5 | IAE with respect to the set-point profile | 4 | Mode 2 | Scenario 0 |
| 6 | Percentage of reduction in the reactor wall temperature relative to a reference | Free of disturbances | Mode 3 | Scenario 1 |

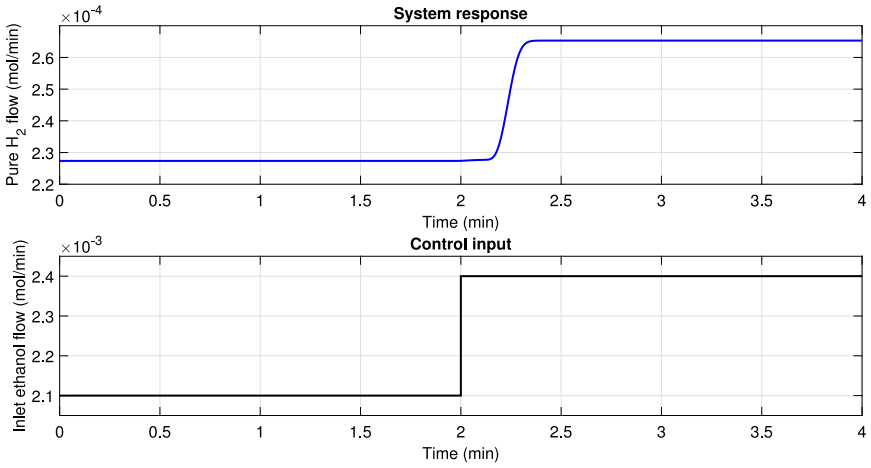


**Fig. 5.** System response to an inlet ethanol molar flow step change (from 0.0021 to 0.0024 mol/min) starting from Mode 1 of normal operating conditions.

- $T_s$ is the sampling time (min), and
- $K_p$, $K_i$, and $K_d$ are the proportional, integral, and derivative gains, respectively.

The values of the parameters $K_p$, $K_i$, and $K_d$ are reported in Table 4. These values were systematically adjusted from initial seed values calculated using the well-known Ziegler–Nichols methodology, based on the system response simulation shown in Fig. 5. These parameters values can be modified by benchmark users to evaluate different PID controller performances. Fig. 6 presents the results of the simulation. The PID controller effectively tracks the hydrogen set-point changes, with transient deviations and stable convergence to the desired values. The inlet ethanol molar flow is adjusted in a stepwise manner to compensate for demand variations, demonstrating smooth control actions without excessive oscillations. The hydrogen set-point changes every 5 min over a 30-min period to demonstrate the system dynamic response and PID controller performance.[2] The performance metric used for evaluating the closed-loop performance is the integral absolute error (IAE), which is approximated using the trapezoidal rule,

$$\mathrm{IAE} = \sum_{k=0}^{M} \left| \frac{e(k) + e(k-1)}{2} T_s \right|, \tag{13}$$

where the upper limit, $M$, is a finite time chosen arbitrarily to ensure that the summation approximates a steady-state value. For this case study, the IAE value was calculated over the total 30 min simulation period, resulting in a value of $7.95\times10^{-5}$ mol. Simulations of the PID controller performance in tracking a set-point profile for pure hydrogen production under Modes 2 and 3 are presented in the supplementary material (Figs. S9 and S10). The controller was operated with the same tuning parameters reported in Table 4. The results reveal a strong dependence of controller effectiveness on the operating mode. In Modes 2 and 3, the closed-loop dynamics exhibit pronounced oscillations and prolonged settling times. Moreover, in some regions of operation the system shows virtually no response to set-point changes, as the control action is limited by saturation of the sole manipulated variable, the inlet ethanol flow. These observations underscore the limitations of fixed-parameter PID control and motivate the use of gain-scheduled or adaptive strategies to preserve stability and performance across varying operating conditions. More importantly, they highlight the advantages of advanced control approaches, such as model predictive control (MPC), which can explicitly account for input and output constraints, adapt to changes in the operating regime, and optimize control performance in ways that conventional PID tuning cannot achieve.

**Table 4**
PID controller parameters.

| Parameter | Value |
|---|---|
| $K_p$ | 1.366 |
| $K_i$ | 0.006 |
| $K_d$ | 0.002 |

### 5.2. Case study 2

The PID controller designed in case study 1 was also used to address control challenge 3. Figs. 7 and 8 illustrate the response of the system to a 10% step and a −20% step change in the gas inlet temperature and pressure, respectively. Both changes were introduced after 5 min of operation time. In both cases, the system reaches the set-point with an initial overshoot, from an initial condition with no inlet ethanol flow (as defined for control challenge 3). Then, the control system rejects the disturbances that occur after 5 min of operation and restores the pure

[2] In real-world microgrid applications, hydrogen demand typically varies on an hourly scale due to stable, yet cyclical, energy consumption patterns influenced by renewable energy availability and load variations.

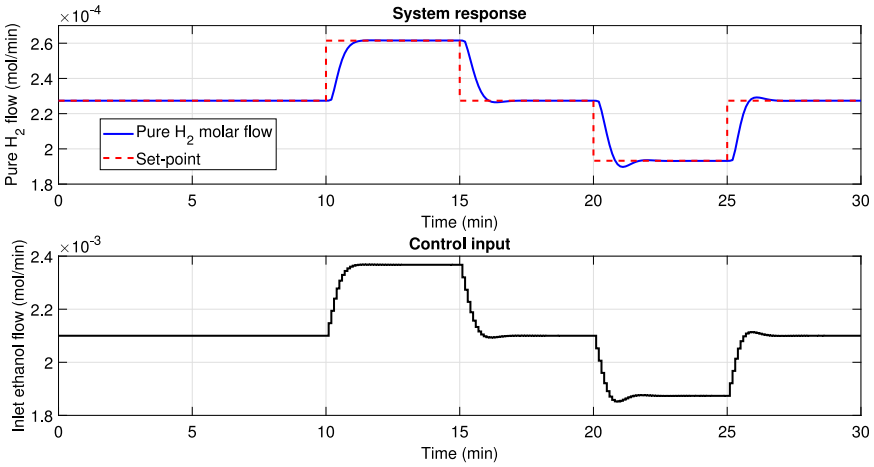


**Fig. 6.** Case study 1. Top: pure hydrogen flow (blue) compared to the set-point trajectory (red dashed line). Bottom: inlet ethanol molar flow (control input).

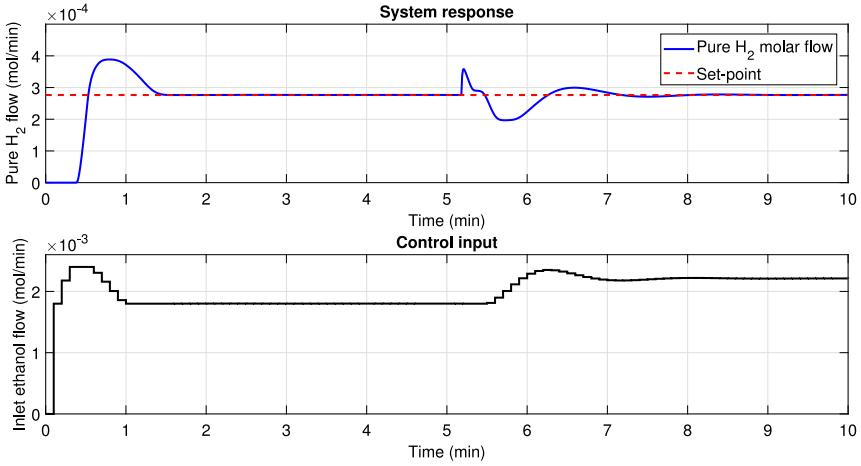


**Fig. 7.** Case study 2. Inlet gas temperature disturbance (10% step change in the inlet gas temperature after 5 min of operation). Top: pure hydrogen flow (blue) and set-point value (red dashed line). Bottom: inlet ethanol molar flow (control input).

hydrogen flow to its set-point value. The IAE calculated with respect to the set-point over the 10 min of operation time are $2.62\times10^{-4}$ mol and $2.48\times10^{-4}$ mol for the gas inlet temperature and gas inlet pressure disturbances, respectively. Although the controller restores the pure hydrogen flow to its set-point, an overshoot exceeding 40% deviation from the set-point is observed in both disturbance scenarios. Such deviations would compromise the stable operation of a fuel cell downstream of the SSMR, since fuel cells require tightly regulated inlet conditions to ensure efficiency and durability. Besides, the system exhibits a shorter settling time for inlet pressure disturbances than for inlet temperature disturbances, even though the applied pressure disturbance was larger. This result indicates that the controller handles pressure variations more smoothly and effectively than temperature fluctuations. While the PID controller tuning could be improved for specific disturbance scenarios, real operation of SSMRs demands controlling multiple variables simultaneously, rejecting any uncertain disturbance, and respecting operational constraints. These requirements further underscore the need for advanced, model-based control strategies to ensure effective and reliable operation of downstream fuel cell units.

## 6. Conclusions

A simulator is presented that provides a benchmark for the control of complex chemical processes, specifically ethanol steam reforming for hydrogen production. A mechanistic model captures the nonlinear dynamics of the reforming and hydrogen separation stages, incorporating chemical reaction kinetics, mass and heat transfer, and process constraints. The model is validated with experimental data at several operating points.

Inclusion of realistic operations, such as inlet fluctuations, catalyst deactivation, and membrane fouling, allows the simulator to mirror real-world conditions. These operational conditions enable researchers to assess the robustness of control strategies under varying conditions, making the simulator a valuable tool for both theoretical studies and practical applications.

The simulator supports a flexible testing environment for research and education, enabling users to explore various control strategies. Although this work illustrated the use of the benchmark simulator with a PID controller, it is equally suitable for advanced control methodologies, such as model predictive control, reinforcement learning, or hybrid schemes combining optimization-based and classical controllers. This flexibility arises from the dynamic model formulation and the open-source, modular implementation, which allows direct access to all process variables, easy integration with optimization libraries, and seamless modification of the control layer.

Performance metrics such as the integral absolute error (IAE) and reduction of ethanol consumption provide a quantitative basis to compare different approaches. Supplementary material and the simulator, developed in the MATLAB® environment, are publicly available at https://github.com/arcmateo/SSMR_Benchmark.git.

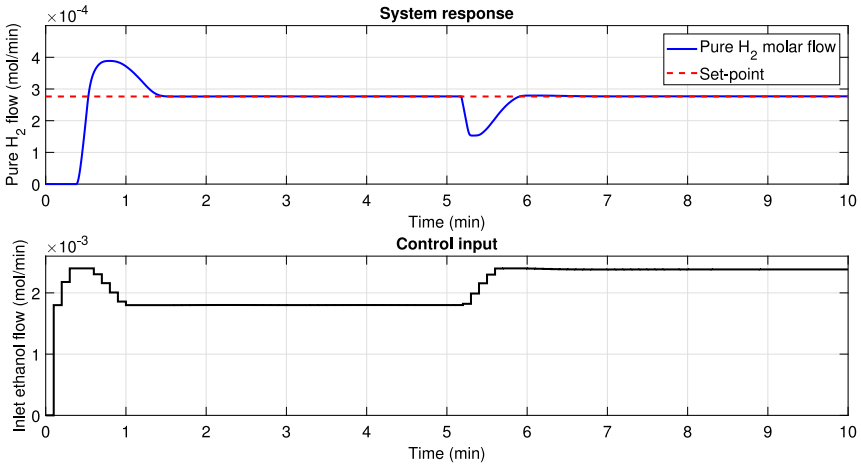


**Fig. 8.** Case study 2. Inlet gas pressure disturbance (−20% step change in the inlet gas pressure after 5 min of operation). Top: pure hydrogen flow (blue) and set-point value (red dashed line). Bottom: inlet ethanol molar flow (control input).

**Table A.1**
Model parameter values. Taken directly or adapted from [25,36].

| Parameter | Symbol | Value | Units |
|---|---|---|---|
| Gas universal constant | $R$ | 8.314 | J/(mol K) |
| Temperature of reference | $T_{\text{ref}}$ | 773 | K |
| Activation energy of reaction | $E_{a,1a}$ | $7.0 \times 10^4$ | J/mol |
| | $E_{a,1b}$ | $1.3 \times 10^5$ | J/mol |
| | $E_{a,1c}$ | $7.0 \times 10^4$ | J/mol |
| | $E_{a,1d}$ | $9.8 \times 10^4$ | J/mol |
| First parameter in (5a) | $\alpha_a$ | 7.96 | dimensionless |
| Second parameter in (5a) | $\beta_a$ | 5.82 | $\text{bar}^{-1}$ |
| Pre-exponential factor of reaction kinetic | $k_{\infty,1a}$ | $2.1 \times 10^4$ | $\text{mol}/(\text{m}^3\ \text{min bar})$ |
| | $k_{\infty,1b}$ | $2.0 \times 10^3$ | $\text{mol}/(\text{m}^3\ \text{min bar})$ |
| | $k_{\infty,1c}$ | $1.9 \times 10^4$ | $\text{mol}/(\text{m}^3\ \text{min bar}^2)$ |
| | $k_{\infty,1d}$ | $2.0 \times 10^5$ | $\text{mol}/(\text{m}^3\ \text{min bar}^4)$ |
| Standard enthalpy of reaction | $\Delta H^\circ_{1a}$ | 64,600 | J/mol |
| | $\Delta H^\circ_{1b}$ | 49,875 | J/mol |
| | $\Delta H^\circ_{1c}$ | −41,166 | J/mol |
| | $\Delta H^\circ_{1d}$ | 109,136 | J/mol |
| Heat transfer coefficient | $U$ | 1500 | $\text{J}/(\text{m}^2\ \text{min K})$ |
| Cross-sectional area | $A$ | $3.8013 \times 10^{-4}$ | $\text{m}^2$ |
| Area per reactor volume for heat transfer | $a$ | 181.82 | $\text{m}^2/\text{m}^3$ |
| Pre-exponential factor of permeation | $P_{e,0}$ | $4.32 \times 10^{-7}$ | $\text{mol}/(\text{min m Pa}^{1/2})$ |
| Apparent activation energy of membrane | $E_{am}$ | $8.8 \times 10^3$ | J/mol |
| Membrane thickness | $\delta$ | $3.0 \times 10^{-5}$ | m |
| Membrane surface area | $\alpha$ | $7.581 \times 10^{-4}$ | $\text{m}^2$ |

## CRediT authorship contribution statement

**Mateo Arcila-Osorio:** Writing – review & editing, Writing – original draft, Methodology, Investigation, Conceptualization. **Francesco Destro:** Writing – review & editing, Methodology, Investigation, Conceptualization. **Carlos Ocampo-Martinez:** Writing – review & editing, Validation, Supervision, Project administration. **Jordi Llorca:** Writing – review & editing, Validation, Supervision, Resources, Formal analysis. **Richard D. Braatz:** Writing – review & editing, Supervision, Resources, Methodology.

## Declaration of competing interest

The authors declare the following financial interests/personal relationships which may be considered as potential competing interests: Mateo Arcila-Osorio reports financial support was provided by Generalitat de Catalunya Ministry of Research and Universities. If there are other authors, they declare that they have no known competing financial interests or personal relationships that could have appeared to influence the work reported in this paper.

## Acknowledgments

This work was supported in part by the Agència de Gestió d'Ajuts Universitaris i de Recerca (AGAUR), Generalitat de Catalunya, Spain under Grant FI SDUR 2023 FISDU 00160 and the Spanish project SEAMLESS: Sustainable learning-based Management of Multi-resource Large-scale Systems (ref. PID2023-148840OB-I00), funded by MCIN/AEI/10.13039/501100011033/FEDER, UE.

## Appendix A. Parameter values

See Table A.1.

## Appendix B. Supplementary data

Supplementary material related to this article can be found online at https://doi.org/10.1016/j.renene.2025.124743.

## References


[1] K. Naseem, F. Qin, F. Khalid, G. Suo, T. Zahra, Z. Chen, Z. Javed, Essential parts of hydrogen economy: Hydrogen production, storage, transportation and application, Renew. Sustain. Energy Rev. 210 (2025) 115196, http://dx.doi.org/10.1016/j.rser.2024.115196.

[2] S. Ahmad, A. Ullah, A. Samreen, M. Qasim, K. Nawaz, W. Ahmad, A. Alnaser, A.M. Kannan, M. Egilmez, Hydrogen production, storage, transportation and utilization for energy sector: A current status review, J. Energy Storage 101 (2024) 113733, http://dx.doi.org/10.1016/j.est.2024.113733.

[3] F. Orecchini, The era of energy vectors, Int. J. Hydrog. Energy 31 (14) (2006) 1951–1954, http://dx.doi.org/10.1016/j.ijhydene.2006.01.015.

[4] I. Staffell, D. Scamman, A. Velazquez Abad, P. Balcombe, P.E. Dodds, P. Ekins, N. Shah, K.R. Ward, The role of hydrogen and fuel cells in the global energy system, Energy Env. Sci. 12 (2019) 463–491, http://dx.doi.org/10.1039/C8EE01157E.

[5] S.O. Jeje, T. Marazani, J.O. Obiko, M.B. Shongwe, Advancing the hydrogen production economy: A comprehensive review of technologies, sustainability, and future prospects, Int. J. Hydrog. Energy 78 (2024) 642–661, http://dx.doi.org/10.1016/j.ijhydene.2024.06.344.

[6] C. Acar, I. Dincer, Comparative assessment of hydrogen production methods from renewable and non-renewable sources, Int. J. Hydrog. Energy 39 (1) (2014) 1–12, http://dx.doi.org/10.1016/j.ijhydene.2013.10.060.

[7] L. Szablowski, M. Wojcik, O. Dybinski, Review of steam methane reforming as a method of hydrogen production, Energy (2025) 134540, http://dx.doi.org/10.1016/j.energy.2025.134540.

[8] B.S. Zainal, P.J. Ker, H. Mohamed, H.C. Ong, I. Fattah, S.A. Rahman, L.D. Nghiem, T.M.I. Mahlia, Recent advancement and assessment of green hydrogen production technologies, Renew. Sustain. Energy Rev. 189 (2024) 113941, http://dx.doi.org/10.1016/j.rser.2023.113941.

[9] J. Xuan, M.K. Leung, D.Y. Leung, M. Ni, A review of biomass-derived fuel processors for fuel cell systems, Renew. Sustain. Energy Rev. 13 (6) (2009) 1301–1313, http://dx.doi.org/10.1016/j.rser.2008.09.027.

[10] M. Chatenet, B.G. Pollet, D.R. Dekel, F. Dionigi, J. Deseure, P. Millet, R.D. Braatz, M.Z. Bazant, M. Eikerling, I. Staffell, P. Balcombe, Y. Shao-Horn, H. Schäfer, Water electrolysis: From textbook knowledge to the latest scientific strategies and industrial developments, Chem. Soc. Rev. 51 (11) (2022) 4583–4762, http://dx.doi.org/10.1039/D0CS01079K.

[11] R. Bhandari, C.A. Trudewind, P. Zapp, Life cycle assessment of hydrogen production via electrolysis – a review, J. Clean. Prod. 85 (2014) 151–163, http://dx.doi.org/10.1016/j.jclepro.2013.07.048, Special Volume: Making Progress Towards More Sustainable Societies through Lean and Green Initiatives.

[12] B. Amini Horri, H. Ozcan, Green hydrogen production by water electrolysis: Current status and challenges, Curr. Opin. Green Sustain. Chem. 47 (2024) 100932, http://dx.doi.org/10.1016/j.cogsc.2024.100932.

[13] H. Ozcan, R.S. El-Emam, S. Celik, B. Amini Horri, Recent advances, challenges, and prospects of electrochemical water-splitting technologies for net-zero transition, Clean. Chem. Eng. 8 (2023) 100115, http://dx.doi.org/10.1016/j.clce.2023.100115.

[14] A.H. Mohammed Abbas, K.K. Cheralathan, E. Porpatham, S.K. Arumugam, Hydrogen generation using methanol steam reforming – catalysts, reactors, and thermo-chemical recuperation, Renew. Sustain. Energy Rev. 191 (2024) 114147, http://dx.doi.org/10.1016/j.rser.2023.114147.

[15] X. Feng, Y. Zhao, Y. Zhao, H. Wang, H. Liu, Q. Zhang, A mini review on recent progress of steam reforming of ethanol, RSC Adv. 13 (34) (2023) 23991–24002, http://dx.doi.org/10.1039/d3ra02769d.

[16] A. Kazmi, T. Sultana, A. Ali, A. Nijabat, G. Li, H. Hou, Innovations in bioethanol production: A comprehensive review of feedstock generations and technology advances, Energy Strat. Rev. 57 (2025) 101634, http://dx.doi.org/10.1016/j.esr.2024.101634.

[17] M. Abdul Kareem Joyia, M. Ahmad, Y.-F. Chen, M. Mustaqeem, A. Ali, A. Abbas, M. Ashraf Gondal, Trends and advances in sustainable bioethanol production technologies from first to fourth generation: A critical review, Energy Convers. Manage. 321 (2024) 119037, http://dx.doi.org/10.1016/j.enconman.2024.119037.

[18] D. Rodríguez-Fontalvo, N. Sánchez, M. Cobo, Sustainable bio-hydrogen production: Assessing economic and environmental implications of a scaled-up industrial bioethanol prototype, Int. J. Hydrog. Energy 74 (2024) 201–213, http://dx.doi.org/10.1016/j.ijhydene.2024.06.109.

[19] J.G. Segovia-Hernández, S. Hernández, E. Cossío-Vargas, M. Juarez-García, E. Sánchez-Ramírez, Green hydrogen production for sustainable development: a critical examination of barriers and strategic opportunities, RSC Sustain. 3 (1) (2024) 134–157, http://dx.doi.org/10.1039/d4su00630e.

[20] G. Squadrito, G. Maggio, A. Nicita, The green hydrogen revolution, Renew. Energy 216 (2023) 119041, http://dx.doi.org/10.1016/j.renene.2023.119041.

[21] G. Zang, E.J. Graham, D. Mallapragada, H2 production through natural gas reforming and carbon capture: A techno-economic and life cycle analysis comparison, Int. J. Hydrog. Energy 49 (2024) 1288–1303, http://dx.doi.org/10.1016/j.ijhydene.2023.09.230.

[22] V.M. García, E. López, M. Serra, J. Llorca, J. Riera, Dynamic modeling and controllability analysis of an ethanol reformer for fuel cell application, Int. J. Hydrog. Energy 35 (18) (2010) 9768–9775, http://dx.doi.org/10.1016/j.ijhydene.2009.09.064, HE (Hydrogen Systems and Materials For Sustainability).

[23] V.M. García, M. Serra, J. Llorca, J. Riera, Design of linear controllers applied to an ethanol steam reformer for PEM fuel cell applications, Int. J. Hydrog. Energy 38 (18) (2013) 7640–7646, http://dx.doi.org/10.1016/j.ijhydene.2012.11.078.

[24] D. Recio-Garrido, C. Ocampo-Martínez, M. Serra-Prat, Design of optimization-based controllers applied to an ethanol steam reformer for hydrogen production, Int. J. Hydrog. Energy 37 (15) (2012) 11141–11156, http://dx.doi.org/10.1016/j.ijhydene.2012.04.117.

[25] M. Serra, C. Ocampo-Martinez, M. Li, J. Llorca, Model predictive control for ethanol steam reformers with membrane separation, Int. J. Hydrog. Energy 42 (4) (2017) 1949–1961, http://dx.doi.org/10.1016/j.ijhydene.2016.10.110.

[26] P. Reyero-Santiago, C. Ocampo-Martinez, R.D. Braatz, Nonlinear dynamical analysis for an ethanol steam reformer: A singular distributed parameter system, in: 2020 59th IEEE Conference on Decision and Control, CDC, 2020, pp. 23–29, http://dx.doi.org/10.1109/CDC42340.2020.9304055.

[27] F.M. Cavalcanti, M. Schmal, R. Giudici, R.M. Brito Alves, A catalyst selection method for hydrogen production through water-gas shift reaction using artificial neural networks, J. Environ. Manag. 237 (2019) 585–594, http://dx.doi.org/10.1016/j.jenvman.2019.02.092.

[28] K. Ghasemzadeh, A. Aghaeinejad-Meybodi, A. Basile, Hydrogen production as a green fuel in silica membrane reactor: Experimental analysis and artificial neural network modeling, Fuel 222 (2018) 114–124, http://dx.doi.org/10.1016/j.fuel.2018.02.146.

[29] W.-H. Chen, C.-Y. Cheng, Y.-K. Chih, R.-Y. Chein, K.-Y.A. Lin, A. Saravanakumar, Hydrogen production optimization from methanol steam reforming using box-behnken design, analysis of variance, and artificial neural network, Int. J. Hydrog. Energy 140 (2025) 1163–1177, http://dx.doi.org/10.1016/j.ijhydene.2024.10.086.

[30] G. Bilgiç, E. Bendeş, B. Öztürk, S. Atasever, Recent advances in artificial neural network research for modeling hydrogen production processes, Int. J. Hydrog. Energy 48 (50) (2023) 18947–18977, http://dx.doi.org/10.1016/j.ijhydene.2023.02.002.

[31] J. Downs, E. Vogel, A plant-wide industrial process control problem, Comput. Chem. Eng. 17 (3) (1993) 245–255, http://dx.doi.org/10.1016/0098-1354(93)80018-I.

[32] S. Goldrick, A. Ştefan, D. Lovett, G. Montague, B. Lennox, The development of an industrial-scale fed-batch fermentation simulation, J. Biotech. 193 (2015) 70–82, http://dx.doi.org/10.1016/j.jbiotec.2014.10.029.

[33] F. Destro, Z.K. Nagy, M. Barolo, A benchmark simulator for quality-by-design and quality-by-control studies in continuous pharmaceutical manufacturing – intensified filtration-drying of crystallization slurries, Comput. Chem. Eng. 163 (2022) 107809, http://dx.doi.org/10.1016/j.compchemeng.2022.107809.

[34] A. Melo, M.M. Câmara, N. Clavijo, J.C. Pinto, Open benchmarks for assessment of process monitoring and fault diagnosis techniques: A review and critical analysis, Comput. Chem. Eng. 165 (2022) 107964, http://dx.doi.org/10.1016/j.compchemeng.2022.107964.

[35] A. Li, C.J. Lim, J.R. Grace, Staged-separation membrane reactor for steam methane reforming, Chem. Eng. J. 138 (1) (2008) 452–459, http://dx.doi.org/10.1016/j.cej.2007.06.024.

[36] I. Uriz, G. Arzamendi, E. López, J. Llorca, L. Gandía, Computational fluid dynamics simulation of ethanol steam reforming in catalytic wall microchannels, Chem. Eng. J. 167 (2) (2011) 603–609, http://dx.doi.org/10.1016/j.cej.2010.07.070, Special Issue - IMRET 11: 11th International Conference on Microreaction Technology.

[37] M. Li, Model Predictive Control for Ethanol Steam Reformers (Master's thesis), Universitat Politècnica de Catalunya, 2014.

[38] R. Koch, E. López, N.J. Divins, M. Allué, A. Jossen, J. Riera, J. Llorca, Ethanol catalytic membrane reformer for direct PEM FC feeding, Int. J. Hydrog. Energy 38 (14) (2013) 5605–5615, http://dx.doi.org/10.1016/j.ijhydene.2013.02.107.

[39] S.C. Chapra, R.P. Canale, Numerical Methods for Engineers, McGraw-Hill Education, 2016.

[40] A. Cifuentes, L. Soler, R. Torres, J. Llorca, Methanol steam reforming over PdZn/ZnAl2O4/Al2O3 in a catalytic membrane reactor: An experimental and modelling study, Int. J. Hydrog. Energy 47 (22) (2022) 11574–11588, http://dx.doi.org/10.1016/j.ijhydene.2022.01.186.